Optics & Laser Technology 149 (2022) 107856

Contents lists available at ScienceDirect

Optics and Laser Technology

journal homepage: www.elsevier.com/locate/optlastec

Low-repetition-rate all-polarization maintaining thulium-doped passively modelocked fiber laser

L.A. Sánchez [a], C. Cuadrado-Laborde [b,*], A. Carrascosa [a], A. Díez [a], J.L. Cruz [a], M.V. Andrés [a]

[a] Departamento de Física Aplicada, ICMUV, Universidad de Valencia, Dr. Moliner 50, Burjassot E-46100, Spain
[b] Instituto de Física Rosario (CONICET-UNR), Blvr. 27 de Febrero 210bis, S2000EZP Rosario, Argentina

ARTICLE INFO

Keywords:
Fiber laser
Polarization maintaining
Thulium-doped
Low-repetition-rate

ABSTRACT

We have developed a passively mode-locked, all-polarization maintaining, low-repetition-rate thulium-doped fiber laser (PM TDFL) emitting at 1951 nm and pumped by an erbium-ytterbium-doped all-fiber laser at 1561 nm. The PM TDFL was developed with a 44.67 m long polarization-maintaining all-fiber resonator Fabry-Perot using a semiconductor saturable absorber mirror at one end and a highly reflective fiber Bragg grating at the other. In this way, transform-limited low-repetition-rate light pulses at 2.3 MHz were generated, with each light pulse having a temporal width of 81 ps, and a spectral width of 50 pm. We have also compared the performance of this laser with a shortened version of this cavity, 6.25 m long, emitting at 15.6 MHz.

1. Introduction

Nowadays, there is an increasing demand for lasers emitting around the 2 μm wavelength for a variety of applications [1]. A major advantage commonly cited is their "eye-safer" nature, in part because vitreous humor is 99 % water, which in turn has strong absorption lines near 2 μm [2,3]. This has also opened the window for various medical applications, such as in dermatology [4], tissue ablation [5], and scalpels development [6]. On the other hand, cutting and welding with 2 μm laser sources has also been demonstrated on polymers, as these materials also exhibit strong absorption in this wavelength range [7]. The unique combination of 2 μm laser sources between their "eye-safer" nature and atmospheric transparency window (about 80 % transmittance at this wavelength) also makes them suitable for laser imaging, detection and ranging (LIDAR) [8,9]. The most popular approach to achieve radiation at 2 μm is to use thulium-doped fibers (TDF), due to their favorable absorption in the infrared *C*-band, which allows direct pumping of fiber lasers within the core [10].

The above applications would benefit from low-repetition-rate mode-locking proposals. However, all-fiber modelocked lasers typically operate above ten megahertz, where the accumulation of nonlinear effects and chromatic dispersion is easier to deal with because the fiber cavity is relatively short. Moreover, low-repetition-rate lasers operating at 2 μm range face an additional problem: the high silica attenuation at this wavelength (typically $>$ 20 dB/km [11]). Of course, we can use pulse-pickers, but this leads to energy loss and back-reflection, which affect the signal-to-noise ratio, and increases the complexity of the system. For this reason, a true modelocked laser with low-repetition-rate is the best choice to overcome these difficulties. So far, some low-repetition-rate TDF modelocked lasers have been presented [12,13,14,15,16,17,18,19,20,21], with repetition rates ranging from 67 kHz [19] to 6.7 MHz [18], but mostly at 2–3 MHz.

The lengthening of a fiber cavity leads often to a different emission regime, since not only power losses but also nonlinearity and chromatic dispersion increase. Thus, we have found dissipative soliton resonance light pulses (DSR) [14–18, 20, 21], whose temporal widths (optical bandwidth) ranges from 780 ps (18.3 nm) [16] to 85 ns (9.4 nm) [21]; i.e., the pulses are strongly chirped. Noise-like pulses (NLP) were also observed in Ref. [18] at 300 ps (5.1 nm), and in Ref. [12] at 4.5 ps (1.56–21 nm) and *h*-like pulses were also found in Ref. [19] at 180–410 ns (10 nm). Finally, standard solitons have also been reported in Ref. [13], but they are unusually wide: 617 ps (4.7 nm), which also contradicts the time-bandwidth limit required for solitons (in this case, a time bandwidth product of 200).

As for the mode-locking mechanism, these proposals are mainly based on nonlinear polarization rotation (NPR) [13], nonlinear optical loop mirror (NOLM) [12,15,16,19,20,21], or nonlinear amplifying loop mirror (NALM) [14,17], with the exception of Ref. [18] which uses single-walled carbon nanotubes as saturable absorber. NPR, NOLM, and NALM strongly depend on the polarization evolution and phase

* Corresponding author at: Instituto de Física Rosario (CONICET-UNR), Blvr. 27 de Febrero 210bis, S2000EZP Rosario, Argentina.
E-mail address: christian.cuadrado@uv.es (C. Cuadrado-Laborde).

https://doi.org/10.1016/j.optlastec.2022.107856
Received 12 July 2021; Received in revised form 16 December 2021; Accepted 3 January 2022
Available online 7 January 2022
0030-3992/© 2022 The Authors. Published by Elsevier Ltd. This is an open access article under the CC BY license (http://creativecommons.org/licenses/by/4.0/).

evolution of the optical pulse in the laser cavity, so it can be easily overdriven in an ultra-long cavity and affected by the environment. For this reason, all of these proposals – except Ref. [14] – use polarization controllers that require multiple adjustments, as well as the fact that self-starts operation are not guaranteed. Moreover, it is common for the operating wavelength to change with pump power and polarization of the resonator, which could be a serious problem in some applications. In contrast, SESAMs are a mature technology approaching half a century of success. They are inherently compatible with polarization-maintaining cavities, while other proposals are not, e.g., those based on polarization evolution (nonlinear optical loop mirrors and similar solutions). Moreover, in SESAMs, the physical length of the saturable-absorber region is small and its contribution to the round-trip time of light in the laser cavity is negligible, resulting in the shortest possible cavities. As a result, SESAMs can be operated at extremely high pulse repetition rates. It is also ideally suited for mode-locking at low repetition-rates, since the saturable absorption is independent of the resonator length.

In this work, we present a low-repetition-rate self-starting all-fiber laser operating at two microns; where mode-locking was achieved by using a SESAM. Thanks to the use of a polarization-maintaining (PM) all-fiber resonator, robustness and insensitivity to harsh environments are ensured. The presence within the cavity of a narrow, high-reflective, fiber Bragg grating also guarantees a narrow spectral bandwidth of the output light pulses, and a fixed operating wavelength, if required. As gain medium, we use a TDF pumped by an erbium-ytterbium doped continuous wave (CW) fiber laser in the infrared *C*-band. Thus, we obtained a low-repetition-rate transform-limited light pulses at 2.3 MHz, with each light pulse having a temporal width of 81 ps, and spectral width of 50 pm at 1951 nm. We have also compared the performance of this laser with a shortened version of this cavity emitting at 15.6 MHz.

2. Experimental setup

The experimental setup is shown in Fig. 1 and consists of two separate blocks: pump unit and oscillator. Let us starts with the former. A high reflective (99.99%) fiber Bragg grating (FBG, $\lambda_B = 1561$ nm and 3 dB bandwidth of 0.26 nm) was used to generate continuous wave emission in the infrared *C*-band. One end of this FBG was fusion-spliced to a 7.5 m double-clad Er/Yb-doped fiber (ErYb 130 from OFS, core/cladding numerical apertures 0.17/0.45, and Yb clad absorption > 1.2 dB/m), which in turn was fusion-spliced to the output of a beam combiner ($\times 6$ input fibers, numerical aperture 0.165, core/cladding diameters 105 ± 3 μm/ 125 ± 2.5 μm). The remarkable core diameter difference between the optical fiber of the beam combiner and the Er/Yb-doped fiber during fusion splicing is sufficient to create a reflectivity of a few percent to form the Fabry-Perot cavity that sustains CW emission at 1561 nm; see the pump block unit [22]. The beam combiner was again fusion-spliced to the output of an optimized GaAs substrate-based quantum well high-power laser diode (LD, from Lumics, emission wavelength at 976 nm and maximum output power of 7700 mW). A thermoplastic jacket (not shown) was attached to the remaining port of the FBG to remove residual light at 976 nm. Finally, an optical circulator (central wavelength 1550 nm) was connected to the output of the beam combiner to avoid back reflections, and thus improve the temporal stability of the CW laser. We also show in Fig. 1 the measured optical spectrum at the output of the pump unit. This pump unit was able to deliver a continuously variable power up to 820 mW at 1561 nm, with a measured slope efficiency of $10.57 \pm 0.08\%$ and laser threshold of 47 mW.

On the other hand, the setup of the oscillator was composed of a typical Fabry-Perot (FP) cavity which we describe below; see Fig. 1, Oscillator block. CW light at 1561 nm from the pump unit entered the FP cavity via a PM FBG with high reflectivity (99%, $\lambda_B = 1951$ nm and -3 dB bandwidth of 0.14 nm), which in turn was fusion-spliced to a 2 m PM TDF (PM-TSF 9/125 from Nufern®, numerical aperture 0.15, cutoff wavelength 1750 nm, and 9 ± 2 dB/m at 1180 nm core absorption). The free end of the PM TDF was fusion-spliced to the common port of a 1550/1950 nm PM wavelength division multiplexer (PM WDM, insertion loss: pass to common < 0.6 dB at 1950 nm and reflect to common < 0.5 dB at 1550 nm). (Strictly speaking a WDM would not be essential in the FP cavity, but we felt it necessary to protect the SESAM of residual pump energy at 1561 nm, especially at high pump powers.) The residual pump power was returned to the cavity by connecting the reflect port of the PM WDM to a dichroic mirror. The pass port of the PM WDM was in turn fusion-spliced to a 38.42 m long PM delay line (PM1550-XP from Nufern®, numerical aperture 0.125, and cut off wavelength 1380 ± 60 nm). The other end of the delay line was fusion-spliced to the input port of a PM optical fiber coupler (PM OFC, 90/10 and with blocked fast axis). The presence of a blocked fast axis element (in this case the PM OFC) guarantees a single polarization state in the oscillator resonator; even when CW pumping provides unpolarized light. Finally, the cavity FP was closed by connecting the 90% port of the PM OFC to a semiconductor saturable absorber mirror (SESAM, from BATOP Optoelectronics, high reflection bandwidth in the 1900–2080 nm range, and

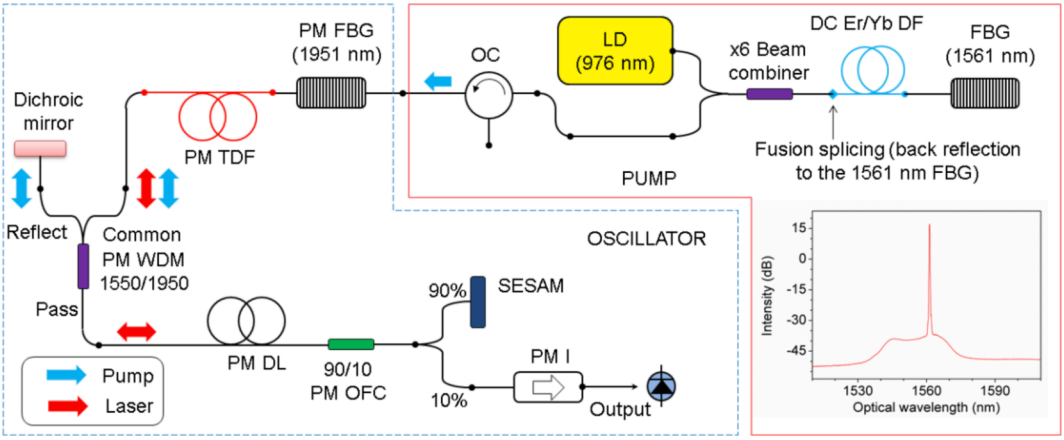

Fig. 1. The figure shows the experimental setup, with the solid lines enclosing the pump unit and the dashed lines enclosing the oscillator. The acronyms used stand for (starting from the top-right and following the different connections): Fiber Bragg Grating (FBG), dual-cladding Er/Yb doped fiber (DC Er/Yb DF), laser diode (LD), optical circulator (OC), polarization-maintaining fiber Bragg grating (PM FBG), polarization-maintaining thulium doped fiber (PM TDF), polarization-maintaining wavelength division multiplexer (PM WDM), polarization-maintaining delay line (PM DL), polarization-maintaining optical fiber coupler (PM OFC), semiconductor saturable absorber mirror (SESAM), and polarization-maintaining isolator (PM I). In addition the spectrum at the output of the CW pump is shown; see the inset in the pump block.

relaxation time constant 10 ps). The output signal from this oscillator was obtained through the 10% port of the PM OFC, which also incorporated two PM optical isolators in tandem (PM I, with center wavelength of 1950 ± 20 nm, and combined 56 dB peak isolation with a 1.2 dB insertion loss) to avoid unwanted reflections at the oscillator. These output light pulses were monitored with a 63 GHz sampling oscilloscope, a 13-GHz real-time oscilloscope, fast InGaAs photodetectors (rise time < 28 ps, fall time < 28 ps, and 0.95 A/W at 2 μm), an optical spectrum analyzer (optical range from 1200 nm to 2400 nm, resolution bandwidth 50 pm), radio frequency (RF) spectrum analyzer (resolution bandwidth 1 Hz, DC to 10 GHz), and a pyroelectric detector for the measurement of the average output power.

The resulting cavity length is 44.67 m, with an estimated average anomalous dispersion parameter of 42.1 ps/nm × km, and a group velocity dispersion of − 85 ps^2/km at 1950 nm; i.e. a total chromatic dispersion per round trip of − 7.6 ps^2 [23]. In the following we compare the results obtained with this long cavity with those obtained with the cavity without PM delay line. This much shorter cavity is 6.25 m long, and has a total chromatic dispersion per round trip of − 1 ps^2.

On the other hand, the attenuation at each round trip of the light pulses is expected to be significant at the operating wavelength of this laser, since the cavity is mainly composed of PM1550-XP, which has an attenuation of 1.0 dB/km at 1550 nm, but of 20 dB/km at 1950 nm. Starting from the SESAM – see the oscillator block in Fig. 1 – the discrete power losses inside the cavity are: −0.4 dB (insertion loss of SESAM), −1.49 dB (90% power of the PM OFC), −0.89 dB (insertion loss of the PM WDM), and since the PM FBG has a high reflectivity, its insertion loss can be neglected. That is 5.6 dB of discrete power loss at each round-trip. To this total discrete power loss must be added the distributed power losses due to the different pigtails of the components (PM 1550), PM DL (PM1550-XP) as well as the active fiber PM TDF (all with a core attenuation of ~ 20 dB/km at 1950 nm). Therefore, the combined discrete-distributed power losses within a full round-trip are 7.4 dB for the long cavity and 5.8 dB for the shorter cavity; i.e., with and without PM delay line.

3. Experimental results and discussion

The long-cavity laser exhibits self-starting stable mode-locking when the LD power is set to 1.6 W. Fig. 2a shows the light pulse train at a frequency of 2.3 MHz obtained at the output, which corresponds to the expected round-trip time for a FP cavity of 44.67 m. We found that the pump power setting is very important at this high anomalous intracavity dispersion, because changing the LD pump power in ± 20 mW turns off the mode-locking regime. This low repetition rate may be the cause of the narrow pumping range, since any change in pump power has a major impact on pulse energy as the repetition rate is low. The quality of this mode-locking regime was tested, by measuring the RF spectrum. As can be seen in Fig. 2(b), the fundamental frequency was 2.3 MHz with a high extinction ratio of up to 65 dB (measured with a resolution bandwidth of 10 Hz). Fig. 2(c) is a wide-span measurement that extends to the 42nd harmonic of the fundamental frequency (measured with a resolution bandwidth of 100 kHz). From the RF spectrum, it is easy to see that the laser was in a stable mode-locking mode. Once mode-locking was started, the stable mode-locking mode could continue as long as the pumping unit was on. This robustness is typical of an all-fiber design that fully retains polarization. In contrast, for the short-cavity setup, the laser was able to start stable mode-locking when the power LD was set to 2.5 W. In this case the output light train is at a consequently higher repetition rate of 15.6 MHz. We have found that adjusting the pump power at this higher frequency is less critical than in the case of the long cavity laser, since any increase in pump power only causes the typical amplitude modulation of the output light train, but without destroying the mode-locking.

The temporal waveform of a single light pulse is shown in detail in Fig. 3(a), as recorded by the digital sampling oscilloscope. The pulse has a full width at half maximum (FWHM) of 81 ps and can be fitted quite well with a secant hyperbolic profile (not shown). Moreover, the sinusoidal ripple after the trailing edge is the consequence of the pole frequency at 14 GHz in the photodetector transfer function. We also measured the output of this laser for the short resonator; i.e., without PM delay line. This waveform can also be seen in Fig. 3(a). The temporal waveform of each light pulse shows no significant change compared to the long cavity resonator; the superposition between the two temporal waveforms (once normalized in intensity) is remarkable; of course, the pulse also has a FWHM of 81 ps. As an experimental precedent, we can mention that in Ref. [24], we obtained similar soliton-like pulses when the length of the resonator was reduced by a factor of two; i.e., from 213 m to 106 m. On the other hand, it has been shown theoretically for soliton mode-locking that the pulse width increases monotonically with the (anomalous) dispersion within the resonator; see for example Fig. 1 (a) in Martinez et al. [25]. It should be emphasized, that these kinds of curves were obtained assuming a small and fixed self-phase modulation (SPM). However, when the cavity is greatly enlarged, this assumption is no longer plausible, since the nonlinear SPM parameter also increases linearly with length. In this case; i.e., with moderate self-phase modulation, the dependence of the pulse width on the (anomalous) dispersion in the cavity is strongly attenuated; see Fig. 2 also in Ref. [25]. Another example is provided by Haus in Fig. 8(a) of Ref. [26], which shows the pulse width as a function of the intracavity dispersion for different values of the SPM parameter. In the present case, when the cavity is shortened from ~ 45 m to ~ 6 m, it means not only lower intracavity dispersion, but also a shift to a curve with a lower SPM parameter. This trend can be clearly seen in Fig. 8(a) of Ref. [26]. Consequently, the pulse width is not expected to change appreciably.

We also measured the optical spectrum of the long-cavity laser, which is shown in Fig. 3b. The spectrum has a double peak, with a − 3 dB bandwidth of 50 pm each. This measurement is below – or very close – to the resolution limit of our OSA (50 pm). We also performed optical spectral measurements for the short cavity; the result is also shown in

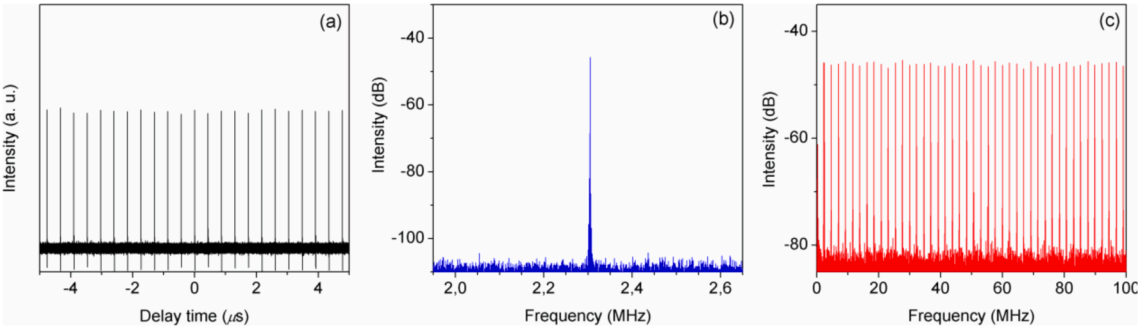

Fig. 2. (a) Oscilloscope trace showing the output train. (b) RF spectrum showing the fundamental frequency. (c) RF spectrum showing from the fundamental frequency up its 42nd harmonic.

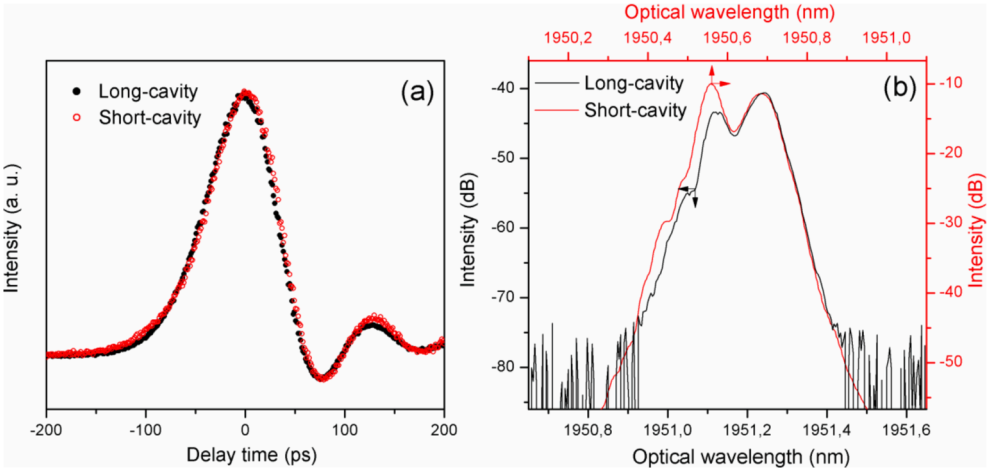

Fig. 3. (a) Oscilloscope traces showing the output light pulses (black solid and red open dots for the long and short cavities, respectively). (b) Optical spectra measured at the output for the long and short cavities (black and red curves, respectively).

Fig. 3b. The spectra are essentially identical at the longer wavelength peak, and overlap with our previous measurement of the long cavity. There is also a small wavelength shift of 0.5 nm between the two spectra, which could be explained by the combined effect between the thermal coefficient for a FBG at this wavelength (~15 pm/°C), plus the wavelength accuracy of our OSA (±0.5 nm at 2 μm). On the other hand, the measured average output powers were 354 μW and 230 μW, for the long and short-cavity setups, respectively; in both cases the measurement were performed after the PM isolator, see Fig. 1. It should be noted that these average output powers include both CW and modelocked pulse emission. However, we can roughly estimate, by fitting each peak individually to a linear scale and calculating the relative areas in the spectrum, that the CW component comprises the 30 % of the measured average power and the pulsed emission the remaining 70 % for the long cavity. For the short cavity, these ratios are 47 % for the CW and 53 % for the pulsed emission. Therefore, the peak powers for the pulsed emission are in the order of 1300 mW and 100 mW for the long and short cavity, respectively. Since this spectral profile has two peaks, we decided to investigate this fact further, keeping in mind a possible CW contribution to the emission of the laser. For this purpose, we use a two microns PM all-fiber pre-amplifier designed by us, capable of delivering up to 1.1 W average power, to study the nonlinear propagation of the amplified emission along a fiber coil. As an example, the nonlinear length of SMF-28 fiber $L_{NL} = 1/(\gamma P_0) \geq 4$ m, for peak power pulses of 500 W, assuming $\gamma = 0.498$ $W^{-1}km^{-1}$ (calculated at 1950 nm). Therefore, strong nonlinear effects are expected when this preamplified output light train is propagated in a 656 m SMF-28 optical fiber, since 656 m $\gg L_{NL}$. As an example, Fig. 4a shows for the short cavity, the normalized spectrum immediately after and before this nonlinear propagation when the pump power of the preamplification stage is increased to the maximum. It is also worth highlighting that the shape of the spectrum does not change after the preamplification stage. From this result, it is clear that the spectral peak at the shorter wavelength shows not significant change, while the peak at the longer wavelength shows the spectral changes normally associated with the various nonlinear processes. Thus, we conclude that the peak at the short-wavelength corresponds to a trace of CW emission, while the peak at the longer wavelength is in fact the spectrum associated with the pulse train. Moreover, we are working on a passive and simple method to easily block the CW emission while preserving the pulsed emission [27]. On the other hand, if we assume a secant hyperbolic profile for the output light pulses, and considering that a bandwidth of 50 pm corresponds to 3.94 GHz at 1950 nm, the time-bandwidth product TBP = 81 × 10^{-12} s × 3.94 × 10^{9} Hz = 0.32; i.e., practically equal to a transform-limited secant hyperbolic profile whose TBP ≥ 0.315. This calculation also give us confidence that we can measure an optical bandwidth of 50 pm; since an optical bandwidth of<50 pm is excluded by the TBP [28]. In a few words, the output light pulses of our long and short cavities are transform-limited secant hyperbolic pulses with 81 ps FWHM temporal width and 50 pm optical bandwidth.

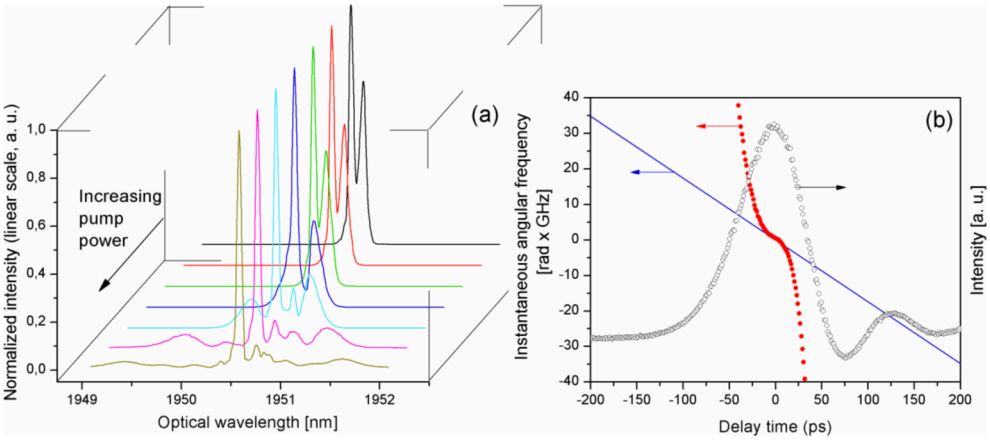

Fig. 4. (a) Spectra at the output of a 656 m SMF-28 coil, using the preamplified short cavity train of pulses as input at different pump powers of the preamplifier stage (3D-waterfall plot). (b) Left ordinate: Measured instantaneous angular frequency and theoretical chirp calculated with Eq. (1) (solid red dots and solid blue line, respectively) for the long cavity train; Right ordinate: Oscilloscope trace showing the light pulse whose instantaneous frequency was retrieved (open dots).

Finally, we measured the instantaneous angular frequency profile of the emitted light pulses using a simple technique that we previously developed [29] and have since successfully applied [30,31]. The technique requires only the measurement of the temporal intensity waveforms at the input and output of the dispersive line together with the knowledge of the GVD of the optical fiber; then the instantaneous angular frequency profile is obtained only by using a single equation in a non-iterative, one-step numerical calculation. As a dispersive line for this technique, we used a 656 m SMF-28 whose GVD at 1950 nm is − 83 ps^2/km [32]. The obtained profile of the instantaneous angular frequency is shown in Fig. 4b, where we have used as an example the long cavity train. It shows a moderately low, but definitely non-zero, slope of − 0.174 rad × GHz/ps. However, the time-bandwidth product suggests a transform limited pulse, which may be at odds with this measurement. For this reason, we decided to investigate the possibility that this chirp is acquired outside the cavity, in the 6 m optical fiber up to the detectors. It is known, that an originally unchirped pulse (i.e., without phase modulation) is chirped after propagating through a fiber with a non-zero GVD. Assuming a Gaussian profile, the chirp degree achieved is given by [33]:

$$\omega(t) = -\frac{\partial\phi(t)}{\partial t} = \frac{sgn(\beta_2)2z/L_D}{1+(z/L_D)^2}\frac{t}{T_0^2}, \quad (1)$$

where $L_D = {T_0}^2/|\beta_2|$the dispersion length, T_0 is the half-width at the $1/e$-intensity point of the temporal waveform − related to the FWHM for a Gaussian pulse by $T_{FWHM} \cong 1.665\ T_0$−, and β_2 is the GVD. The result can also be seen in Fig. 4b, since both instantaneous angular frequency profiles have the same slope in the central part of the pulse. We conclude that our light pulses are chirp-free immediately after the cavity. This behavior was also replicated by the short cavity pulses with no appreciable differences. In summary, long and short cavities produce virtually identical light pulses, except for the repetition rate and average power of course.

4. Conclusions

We have developed a low-repetition-rate passively mode-locked PM-TDFL, pumped by a *C*-band CW erbium-ytterbium doped all-fiber laser. A low-repetition-rate train of transform-limited light pulses was generated at 2.3 MHz was obtained, with each light pulse having a temporal width of 81 ps and a spectral width of 50 pm. We also compare the performance of this laser with a shortened version of this cavity, 6.25 m long, emitting at 15.6 MHz, with no appreciable differences in the output light pulses. This laser differs from previously presented lasers in its unique combination of transform-limited clean pulses with a low-repetition-rate and narrow spectral linewidth. We can envision several applications where this combination could be useful, from LIDAR to material-selective processing where the target material has significantly higher absorption at a given wavelength than adjacent materials.

Declaration of Competing Interest

The authors declare that they have no known competing financial interests or personal relationships that could have appeared to influence the work reported in this paper.

Acknowledgements

This work was supported in part by the European Union, project IPN-Bio (Ref.: H2020-MSCA-RISE-2019-872049), and by the *Generalitat Valenciana* of Spain (Ref.: PROMETEO/2019/048). C. Cuadrado-Laborde acknowledges the financial support from project PIP 2015-0607 (CONICET, Argentina).

References

[1] C.W. Rudy, M.J.F. Digonnet, R.L. Byer, Advances in 2-μm Tm-doped mode-locked fiber lasers, Opt. Fiber Technol. 20 (6) (2014) 642–649.
[2] J.E. Bertie, Z. Lan, Infrared Intensities of Liquids XX: The intensity of the OH stretching band of liquid water revisited, and the best current values of the optical constants of H2O(l) at 25°C between 15,000 and 1 cm^{-1}, Appl. Spectrosc. 50 (8) (1996) 1047–1057.
[3] K. Scholle, S. Lamrini, P. Koopmann, P. Fuhrberg, "2 μm laser sources and their possible applications", Frontiers in Guided Wave Optics and Optoelectronics, B. Pal (Ed.), INTECH Open Access Publisher, p. 471 (2010).
[4] K.D. Polder, S. Bruce, Treatment of melasma using a novel 1,927-nm fractional thulium fiber laser: a pilot study, Dermatol. Surg. 38 (2012) 199–206.
[5] D. Theisen, V. Ott, H. W. Bernd, V. Danicke, R. Keller, R. Brinkmann, CW high power IR-laser at 2μm for minimally invasive surgery, in: Therapeutic Laser Applications and Laser-Tissue Interactions, R. Steiner, ed., Vol. 5142 of Proc. SPIE (Optical Society of America, 2003), paper 5142_96.
[6] X. Xie, Q. Xu, W. Hu, W. Zhang, Q. Dai, J. Chen, J. Deng, H. Song, S.-X. Wang, A brief review of 2 μm laser scalpel, in: 2020 IEEE 5th Optoelectronics Global Conference (OGC), 2020, pp. 63–67.
[7] I. Mingareev, F. Weirauch, A. Olowinsky, L. Shah, P. Kadwani, M. Richardson, Welding of polymers using a 2 μm thulium fiber laser, Opt. & Laser Technol. 44 (2012) 2095–2099.
[8] B.J. Orr, Infrared LIDAR Applications in Atmospheric Monitoring, John Wiley & Sons, 2017.
[9] G.J. Koch, J.Y. Beyon, F. Gibert, B.W. Barnes, S. Ismail, M. Petros, P.J. Petzar, J. Yu, E.A. Modlin, K.J. Davis, U.N. Singh, Side-line tunable laser transmitter for differential absorption LIDAR measurements of CO_2: design and application to atmospheric measurements, Appl. Opt. 47 (2008) 944–956.
[10] Z. Quan, C. Gao, H. Guo, N. Wang, X. Cui, Y. Xu, B. Peng, W. Wei, 400 mW narrow-linewidth Tm-doped silica fiber laser output near 1750nm with volume Bragg grating, Sci. Rep. 5 (2015) 12034.
[11] https://www.thorlabs.com/thorproduct.cfm?partnumber=SM2000.
[12] J. Li, Z. Zhang, Z. Sun, H. Luo, Y. Liu, Z. Yan, C. Mou, L. Zhang, S.K. Turitsyn, All-fiber passively mode-locked Tm-doped NOLM-based oscillator operating at 2-μm in both soliton and noisy-pulse regimes, Opt. Express 22 (7) (2014) 7875, https://doi.org/10.1364/OE.22.007875.
[13] T. Wang, W. Ma, Q. Jia, Q. Su, P. Liu, P. Zhang, *"Passively mode-locked fiber lasers based on nonlinearity at 2-μm band,"* in IEEE J. of Sel. Top, Quantum Electron. 24 (2018) 1–11.
[14] L. Han, T. Wang, B. Chen, W. Ma, Y. Zhao, H. Jiang, Square-wave pulse in 2-μm all-polarization-maintaining passively mode-locked fiber laser, Opt. Eng. 59 (2020), 116107.
[15] T. Du, W. Li, Q. Ruan, K. Wang, N. Chen, Z. Luo, 2 μm high-power dissipative soliton resonance in a compact σ-shaped Tm-doped double-clad fiber laser, Appl. Phys. Express 11 (5) (2018) 052701, https://doi.org/10.7567/APEX.11.052701.
[16] H. Wang, T. Du, Y. Li, J. Zou, K. Wang, F. Zheng, J. Fu, J. Yang, H. Fu, Z. Luo, 2080 nm long-wavelength, high-power dissipative soliton resonance in a dumbbell-shaped thulium-doped fiber laser, Chin. Opt. Lett. 17 (2019), 030602.
[17] Y. Wu, J.-R. Tian, Z. Dong, C. Liang, Y.-R. Song, Generation of Two Dissipative Soliton Resonance Pulses in an All-Anomalous-Dispersion Regime Thulium-Doped Fiber Laser, IEEE Photon. J. 11 (6) (2019) 1–8.
[18] Q.-.-Q. Wang, T. Chen, M. Li, B. Zhang, Y. Lu, K.P. Chen, All-fiber ultrafast thulium-doped fiber ring laser with dissipative soliton and noise-like output in normal dispersion by single-wall carbon nanotubes, Appl. Phys. Lett. 103 (2013), 011103.
[19] J. Zhao, L. Li, L. Zhao, D. Tang, D. Shen, L. Su, Tunable and switchable harmonic h-shaped pulse generation in a 3.03 km ultralong mode-locked thulium-doped fiber laser, Photon. Res. 7 (2019) 332–340.
[20] J. Zhao, D. Ouyang, Z. Zheng, M. Liu, X. Ren, C. Li, S. Ruan, W. Xie, 100 W dissipative soliton resonances from a thulium-doped double-clad all-fiber-format MOPA system, Opt. Express 24 (11) (2016) 12072, https://doi.org/10.1364/OE.24.012072.
[21] B. Ibarra-Escamilla, M. Duran-Sanchez, B. Posada-Ramirez, H. Santiago-Hernandez, R. Ivan Alvarez-Tamayo, D.S. de la Llave, M. Bello-Jimenez, E. A. Kuzin, Dissipative soliton resonance in a thulium-doped all-fiber laser operating at large anomalous dispersion regime, IEEE Photon. J. 10 (5) (2018) 1–7.
[22] J. del Valle-Hernandez, Y.O. Barmenkov, S.A. Kolpakov, J.L. Cruz, M.V. Andres, A distributed model for continuous-wave erbium-doped fiber laser, Opt. Commun. 284 (2011) 5342–5347.
[23] A. Rampur, Y. Stepanenko, G. Stępniewski, T. Kardaś, D. Dobrakowski, D.-M. Spangenberg, T. Feurer, A. Heidt, M. Klimczak, Ultra low-noise coherent supercontinuum amplification and compression below 100 fs in an all-fiber polarization-maintaining thulium fiber amplifier, Opt. Express 27 (24) (2019) 35041, https://doi.org/10.1364/OE.27.035041.
[24] C. Cuadrado-Laborde, J.L. Cruz, A. Díez, M.V. Andrés, Sub-picosecond ultra-low frequency passively mode-locked fiber laser, Appl. Phys. B 122 (2016) 273.
[25] O.E. Martinez, R.L. Fork, J.P. Gordon, Theory of passively mode-locked lasers including self-phase modulation and group-velocity dispersion, Opt. Lett. 9 (1984) 156–158.
[26] H.A. Haus, *"Mode-locking of lasers,"* IEEE, J. Sel. Topics in Quantum Electron. 6 (6) (2000) 1173–1185.
[27] E. Hernández-Escobar, M. Bello-Jiménez, O. Pottiez, B. Ibarra-Escamilla, R. López-Estopier, M. Duran-Sánchez, M.A. García Ramírez, E.A. Kuzin, Elimination of continuous-wave component in a figure-eight fiber laser based on a polarization asymmetrical NOLM, Laser Phys. 27 (2017), 075105.
[28] A.E. Siegman, Lasers, University Science Books, 1986.

[29] C. Cuadrado-Laborde, A. Carrascosa, P. Pérez-Millán, A. Díez, J.L. Cruz, M. V. Andrés, Phase recovery by using optical fiber dispersion, Opt. Lett. 39 (2014) 598–601.
[30] C. Cuadrado-Laborde, M. Brotons-Gisbert, G. Serafino, A. Bogoni, P. Pérez-Millán, M.V. Andrés, Phase recovery by using optical fiber dispersion and pulse pre-stretching, Appl. Phys. B 117 (2014) 1173–1181.
[31] C. Cuadrado-Laborde, I. Armas-Rivera, A. Carrascosa, E.A. Kuzin, A. Díez, M. V. Andrés, Instantaneous frequency measurement of dissipative soliton resonance light pulses, Opt. Lett. 41 (2016) 5704–5707.
[32] P. Ciąćka, A. Rampur, A. Heidt, T. Feurer, M. Klimczak, Dispersion measurement of ultra-high numerical aperture fibers covering thulium, holmium, and erbium emission wavelengths, J. Opt. Soc. Am. B 35 (2018) 1301–1307.
[33] G.P Agrawal, Nonlinear fiber Optics, 6th Ed. Academic Press.